Lithium-Battery Anode Gains Additional Functionality for Neuromorphic Computing through Metal–Insulator Phase Separation

Juan Carlos Gonzalez-Rosillo, Moran Balaish, Zachary D. Hood, Neel Nadkarni, Dimitrios Fraggedakis, Kun Joong Kim, Kaitlyn M. Mullin, Reto Pfenninger, Martin Z. Bazant, and Jennifer L. M. Rupp*

Specialized hardware for neural networks requires materials with tunable symmetry, retention, and speed at low power consumption. The study proposes lithium titanates, originally developed as Li-ion battery anode materials, as promising candidates for memristive-based neuromorphic computing hardware. By using ex- and in operando spectroscopy to monitor the lithium filling and emptying of structural positions during electrochemical measurements, the study also investigates the controlled formation of a metallic phase ($Li_7Ti_5O_{12}$) percolating through an insulating medium ($Li_4Ti_5O_{12}$) with no volume changes under voltage bias, thereby controlling the spatially averaged conductivity of the film device. A theoretical model to explain the observed hysteretic switching behavior based on electrochemical nonequilibrium thermodynamics is presented, in which the metal-insulator transition results from electrically driven phase separation of $Li_4Ti_5O_{12}$ and $Li_7Ti_5O_{12}$. Ability of highly lithiated phase of $Li_7Ti_5O_{12}$ for Deep Neural Network applications is reported, given the large retentions and symmetry, and opportunity for the low lithiated phase of $Li_4Ti_5O_{12}$ toward Spiking Neural Network applications, due to the shorter retention and large resistance changes. The findings pave the way for lithium oxides to enable thin-film memristive devices with adjustable symmetry and retention.

Neural network (NN) algorithms[1–4] play an increasingly important and widespread role in modern computing. Despite advances in software, however, there remains a fundamental challenge in hardware, since it is inherently awkward and inefficient to simulate the brain—a group of neurons connected by weighted connections—on traditional transistor-based hardware, which amount to a collection of binary switches. This fundamental incompatibility is compounded by well-known problems with transistor-based architectures[5–7] due to inescapable quantum effects (tunneling), nanoscale heat management, and difficulty building devices into the third dimension.

In response to the growing prevalence of NN algorithms, there is increasing interest in developing "neuromorphic" hardware that mimics the brain and thus would naturally complement NN algorithms, enabling faster and more efficient execution. One promising approach is based on "memristors", or circuit elements whose resistive state can be switched under high electric fields to store information, either by ionic migration[5] or due to a phase-change.[8,9] For NN application, memristive devices must meet a number of requirements, admitting certain variability at the device level:[10,11] µs-ms switching timescales, relatively long state retention $\approx 10^5$s, and large number of addressable resistive states, which implies large resistance ratios ($R_{off}/R_{on} > 500$). Memristors are also central to research into Resistive Random Access

Dr. J. C. Gonzalez-Rosillo, Dr. M. Balaish, Dr. Z. D. Hood, Dr. K. J. Kim, K. M. Mullin, Dr. R. Pfenninger, Prof. J. L. M. Rupp
Electrochemical Materials
Department of Materials Science and Engineering
Massachusetts Institute of Technology
77 Massachusetts Av., 02139 Cambridge, MA, USA
E-mail: jrupp@mit.edu
Dr. N. Nadkarni, D. Fraggedakis, Prof. M. Z. Bazant
Department of Chemical Engineering
Massachusetts Institute of Technology
77 Massachusetts Av., 02139 Cambridge, MA, USA

Dr. R. Pfenninger
Electrochemical Materials
Swiss Federal Institute of Technology
8093 Zurich, Switzerland
Prof. M. Z. Bazant
Department of Mathematics
Massachusetts Institute of Technology
77 Massachusetts Av., 02139 Cambridge, MA, USA
Prof. J. L. M. Rupp
Electrochemical Materials
Department of Electrical Engineering and Computer Science
Massachusetts Institute of Technology
77 Massachusetts Av., 02139 Cambridge, MA, USA

**ADVANCED
SCIENCE NEWS**

www.advancedsciencenews.com

**ADVANCED
MATERIALS**

www.advmat.de

Memories (RRAM)[12] and even long-term data storage.[13] The requirements in these applications are different: ≈ns resistive switching, much longer state retention (>10 years), and high cycle-to-cycle reproducibility (<1%). However, memristors for storage applications do not need such a large number of addressable resistance states (resistance ratios < 10).

The largest two categories of memristive devices—valence change memories and electrochemical metallization memories—rely on creation, annihilation, and motion of ions and defects through ionic conductors under a bias (which is used to control resistive state). Valence change memories are based on transition metal oxides whose resistive state depends on the redistribution of bulk O^{2-} and O^{2-} vacancies under bias (and resulting reduced metal cations).[5,14–20] Typical diffusivity values for state-of-the-art switching oxides ($SrTiO_3$,[21] TiO_2[22] and TaO_x[23,24]) are 10^{-15}–10^{-13} cm^2 s^{-1} at ambient temperature. In contrast, electrochemical metallization memories[25] are based on electrochemically active metal electrodes. Under bias, mobile cations, such as Ag^+ or Cu^{2+}, are transported through the interstitials of a solid electrolyte (usually a chalcogenide) forming and dissolving metallic filaments via redox reactions at the electrodes. Typical diffusivities range around 10^{-4}–10^{-7} cm^2 s^{-1}[26] in $Cu_{2-\alpha}S$ electrolyte films, which result in low switching currents under applied voltages.[27–30] Both classes of memristive devices rely on filament formation, a highly complex process still under investigation. Although empirical operation protocols have been devised for voltage and current versus time, it is difficult to predict the size and number of formed filaments, which hinders reversibility, accuracy and symmetry. This, in turn, can be detrimental for neuromorphic devices, where analog switching with finely adjustable resistive states is desirable.

Li-ion intercalation oxides are an attractive new class of functional materials for memristive devices.[31] Relative to valence change memories, Li-ion intercalation oxides have at least 2 orders of magnitude larger diffusivities (10^{-9}–10^{-11} cm^2 s^{-1}).[32–34] Additionally, a metal–insulator transition (MIT) can be easily and drastically tuned by changing the Li content of the material. More specifically, by tuning the overall lithium concentration in Li_xCoO_2 films, one can change the average conductance of the device by several orders of magnitude across the MIT.[35–39] However, the dynamics for creating new stable electronic states in Li_xCoO_2 devices are still under debate, and phase separation associated with the MIT leads to complex switching behavior.[36,40]

Other alternative and promising compounds for use in future neuromorphic devices are doped lithium-spinels $Li_{1-x}B_2O_{4-\delta}$. The transition metal ion, B, can be modulated in its electronic valence and spin state through the stoichiometries of both Li and B structural sites. In fact, the choice of B site cation thus has a significant effect on the electronic structure, and therefore can enable MIT that effects the magnitude and shape of resistive switching behavior. One remarkable ability of Li-spinels is that the Li ion and transition metal can occupy both the tetrahedral and octahedral sites, depending on the valence state, ionic radii and d-band electronic count of the transition metal. In contrast to binary oxides and perovskites, Li-spinels offer a wider range of conditions to manipulate the crystal stabilization energies and to tailor phase change

dynamics for inducing metal–insulator transitions. To date, there has been only one report on the switching characteristics for the Li-spinel $LiFe_5O_8$.[41] Besides that, the scarce literature on Li-based memristor architectures has focused on layered hexagonal Li_xCoO_2,[36–39,42] layered $LiNbO_x$[43–46] and perovskite $LiLaTiO_3$.[47]

In this work, we propose $Li_{4+3x}Ti_5O_{12}$ as a new material for neuromorphic computing. Its ability to undergo metal–insulator transition under applied bias (electric field), allows for changes in its intrinsic switching characteristics, such as retention, switching dynamics and resistive ratio. Furthermore, $Li_{4+3x}Ti_5O_{12}$ develops very small strains for $x \in (0, 1)$, and thus, in contrast to Li_xCoO_2 and other layered oxides, can be characterized as a zero-strain material[48] with a cubic and therefore isotropic (spinel) structure.[49–51] Structurally, this phenomenon occurs due to the small interatomic distances between the 8a sites, that are filled in the stoichiometric $Li_4Ti_5O_{12}$ phase, and the 16c sites, filled in the highly lithiated $Li_7Ti_5O_{12}$.[52] Overall, $Li_{4+3x}Ti_5O_{12}$ can be operated as zero-strain memristor with isotropic electronic state changes and transport characteristics (in- and cross-plane properties) allowing for high flexibility for designing memristive devices with superior cyclability. There is still a debate on whether a solid solution through intermediate phases is formed, or there is a two-phase coexistence between $Li_4Ti_5O_{12}$ and $Li_7Ti_5O_{12}$,[52,53] as assumed in Li-ion battery modeling and synthesis of both end members with controlled stoichiometry in film form is challenging.[54,55] Despite the recent impact of lithium cobaltites on neuromorphic computing and initial modeling their metal–insulator transitions,[40] lithium titanates have yet to be explored as functional material for memristors, focusing on their unique electronic properties and strain-free phase separation under large electric fields.

Here, we studied and exploited the fundamental chemical and structural characteristics of lithium titanate for the development of neuromorphic computing architectures. We used in-depth spectroscopic analysis to understand the fundamental mechanism linking switching behavior and MIT of lithium oxide materials. We translated our understanding into materials and devices, using new processing capabilities that allow us to uniquely set, during deposition, the lithium stoichiometry to that of spinel $Li_4Ti_5O_{12}$ phase or the rock-salt $Li_7Ti_5O_{12}$ phase. This synthesis methodology adds new capabilities to define the original phase and structure before and after switching for lithium oxide films, which has not been studied in earlier reports on Li_xCoO_2 or any other lithium-based memristive device. Next, we propose a thermodynamic model that interprets the metal–insulator transition as an electric field-induced phase separation process between $Li_4Ti_5O_{12}$ and $Li_7Ti_5O_{12}$. We then apply the model to qualitatively explain our experimental findings, providing further insights into the origin of the large changes in conductivity upon applied bias. Finally, we propose material requirements for lithium-based neuromorphic architectures.

We first explored the effect of lithiation degree established in the initial growth of lithium titanate films by pulsed laser deposition. Two-terminal structures of Li-titanate thin films sandwiched between Pt metal electrodes were fabricated in order to exemplify their resistive switching capabilities,

Figure 1a. Various top 250 μm × 250 μm Pt microelectrodes for cross geometries on a Li-titanate thin film are shown, Figure 1b. We deposited either the insulating spinel $Li_4Ti_5O_{12}$ or conducting rock-salt $Li_7Ti_5O_{12}$ phase, building two types of switching devices. We control the phase as in ref. [56]. We carried out a multilayer deposition, including an internal lithiation reservoir (Li_3N), at moderate temperatures to form a single phase. The number of layers of Li_3N determines the amount of lithium in the film, in the stabilizing either rock-salt $Li_7Ti_5O_{12}$ phase or the insulating spinel $Li_4Ti_5O_{12}$. Controlling lithium stoichiometry and manufacturing of highly lithiated phases (as required for the $Li_7Ti_5O_{12}$) remains still challenging in the oxide Li film synthesis community, where direct deposition of a $Li_7Ti_5O_{12}$ film has not yet been reported. Using the synthesis with an additional Li_3N source allows us to uniquely deposit both lithium titanate phases of low and high lithium content as model thin-film structures for future memristive switches.

We analyzed the cross-sectional SEM images of 100 nm thin $Li_4Ti_5O_{12}$ and $Li_7Ti_5O_{12}$ films integrated with a Pt bottom electrode on Si_3N_4/Si chips. The $Li_7Ti_5O_{12}$ film was dense, flat, and continuous with no evidence of porosity. We judge the synthesis approach to a be successful method to introduce higher lithiation degree in the films, with no need of complex
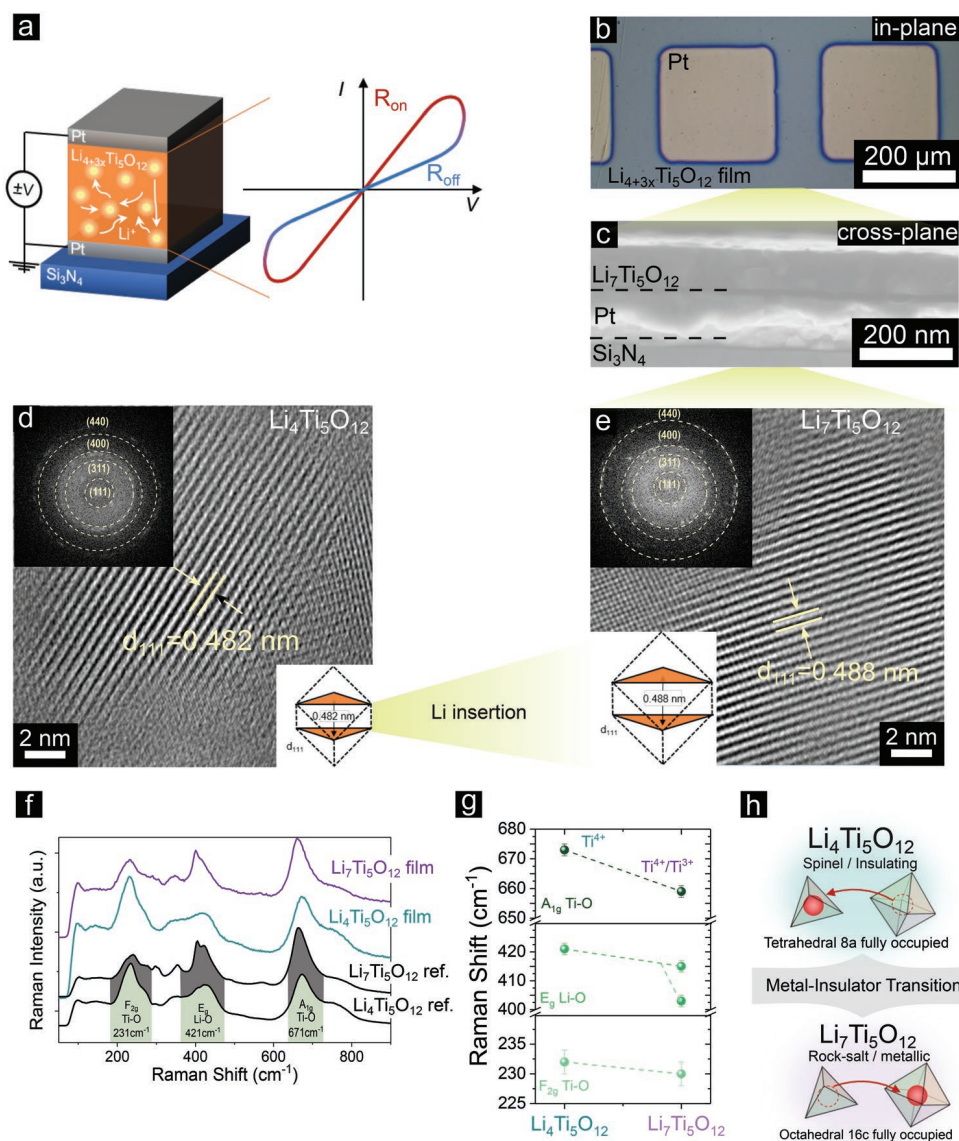

Figure 1. a) Schematic of the Li-titanate device with memristive functionalities. b) Top view image of the $Li_{4+3x}Ti_5O_{12}$ devices with Pt electrodes. c) Cross-sectional SEM image of a $Li_7Ti_5O_{12}$ thin film deposited by pulsed laser deposition on Pt/Si_3N_4/Si substrates. d) HRTEM of a (111) oriented grain in a $Li_4Ti_5O_{12}$ film. Inset shows Fast Fourier Transform (FFT) of the grain. e) HRTEM of a (111) oriented grain in a $Li_7Ti_5O_{12}$ film. Inset shows Fast Fourier Transform (FFT) of the grain. f) Raman spectra of thin film of $Li_4Ti_5O_{12}$ and $Li_7Ti_5O_{12}$ films deposited on Pt/Si_3N_4/Si substrates acquired at 10 mW with a 532 nm wavelength laser. Powder reference patterns ($Li_4Ti_5O_{12}$) as well as highly lithiated PLD target ($Li_{7.1}Ti_5O_{12}$) are included. g) Detail analysis of peak position for the three Raman active bands for the $Li_4Ti_5O_{12}$ and $Li_7Ti_5O_{12}$. A shift toward lower wave numbers in the A_{1g} Ti-O band, indicating a reduction of Ti valence states, and a peak splitting in the E_g Li-O bands are observed in the highly lithiated film. h) Schematic representing the position of the mobile Li ions in the structure in the $Li_4Ti_5O_{12}$ films (tetrahedral 8a positions) versus in $Li_7Ti_5O_{12}$ (octahedral 16c positions).

**ADVANCED
SCIENCE NEWS**
www.advancedsciencenews.com

**ADVANCED
MATERIALS**
www.advmat.de

electrochemical cell arrangement, Figure 1b,c. Reducing the lithium concentration to the $Li_4Ti_5O_{12}$ phase in synthesis does not significantly alter the film microstructure which we detail in Supporting Information Figure S1. X-Ray diffraction (XRD) confirms the $Fd\bar{3}m$ space group for both films with nearly identical lattice parameters for both lithium titanate phases, see Supporting Information Figure S2. Thus, we conclude lithium titanate is a "zero-strain" lithium oxide, with no strong volumetric change upon phase change for the films. Additionally, we conclude that phase differentiation is nearly impossible to achieve via XRD, in accordance to earlier reports.[48,57] To gain further insight into the macroscopic and structural differences of both film phases for the switching devices, we turned to high resolution transmission electron (HRTEM). The microscopic analysis shows in both cases polycrystalline films with comparable average crystallite size of 18 ± 10 nm for $Li_4Ti_5O_{12}$ and 21 ± 10 nm for $Li_7Ti_5O_{12}$. In the lower lithiated $Li_4Ti_5O_{12}$ film, an inter-planar spacing in (111) oriented grains of 0.482 nm is found, Figure 1d. The reduced fast Fourier transform suggests a spinel structure in the $Li_4Ti_5O_{12}$ phase, see inset in Figure 1d. In contrast, for the $Li_7Ti_5O_{12}$ film at deposition, the interplanar distance in (111) oriented grains is slightly enlarged to 0.488 nm, Figure 1e. The reduced fast Fourier Transform suggests a rock-salt-like crystal structure in the $Li_7Ti_5O_{12}$ phase, combined with slight elongation along the (111) direction, see inset in Figure 1e. This elongation is a strong indication of a successful deposition at a larger lithium concentration per unit cell and points to the $Li_7Ti_5O_{12}$ phase for this film.

To ultimately confirm the phases, we turned to Raman spectroscopy, Figure 1f: Three main Raman active bands are observed for $Li_4Ti_5O_{12}$ positioned at 676, 421, and 231 cm^{-1}, which are attributed to the symmetric stretching vibration mode A_{1g} of the Ti$-$O bond, the asymmetric stretching mode E_g of the Li$-$O bond and the bending vibration mode F_{2g} of the Ti-O, respectively. These can be attributed to a full development of the insulating $Li_4Ti_5O_{12}$ phase by comparison (and agreement) with Ref. [58]. For $Li_7Ti_5O_{12}$ films, the main Raman active bands are located with red shifts at 662, a peak splitting at 415 and 403, and 230 cm^{-1} and the appearance of a new peak 340 cm^{-1}. Peak splitting at 415 and 403 cm^{-1} and an extra vibration at 340 cm^{-1} indicate the successful synthesis of the metallic conducting phase $Li_7Ti_5O_{12}$. We assign the splitting and extra vibration mode of the $Li_7Ti_5O_{12}$ film to the transfer of its lithium ions from the Wyckoff 8a tetrahedral positions to the 16c octahedral positions. In case of the $Li_4Ti_5O_{12}$ films, the 16c octahedral Wyckoff positions are expected to be empty leading to an increased electronic band gap and therefore, resulting in an insulating behavior in accordance to Refs. [48,59–61] for pellets and Refs. [61] for films. This is further supported by the strong red shift of 14 cm^{-1} for the A_{1g} vibration mode of the Ti$-$O bond for the $Li_7Ti_5O_{12}$, when compared to the $Li_4Ti_5O_{12}$ film, which indicates a reduction of Ti^{4+} to Ti^{3+}, Figure 1g. The Raman spectrum of our $Li_4Ti_5O_{12}$ film matches perfectly with the $Li_4Ti_5O_{12}$ reference measured on $Li_4Ti_5O_{12}$ powders, see Refs. [48,58–60,62]. The higher lithiated film shows an almost identical match to the $Li_7Ti_5O_{12}$ ceramic pellet used for synthesis, and it is in line with in situ electrochemical cells used in Raman experiments to actively lithiate with a chemical lithium source,[48] Figure 1h. We conclude that to the best of our

knowledge it is first time that the $Li_7Ti_5O_{12}$ phase has directly been synthesized in thin film form, which we credit to the use of the new Li_3N synthesis route to overlithiate. Further experimental evidences and discussion of the as-deposited $Li_4Ti_5O_{12}$ and $Li_4Ti_5O_{12}$ phases investigated by Electron Energy Loss Spectroscopy (EELS) and Electrochemical Impedance Spectroscopy can be found in the Supporting Information.

In summary, lithium titanate films of $Li_4Ti_5O_{12}$ and $Li_7Ti_5O_{12}$ were successfully deposited as either insulating or conductive components for two-terminal memristive device structures. We actively manipulate the metal-to-insulator transition of lithium titanate at PLD deposition using an internal lithiation (based on a new synthesis chemistry via a Li_3N source) to define over the miscibility gap the respective phase. It is to be noted that we add here a new aspect to lithium memristive structures, clearly pre-defining the phases and electronic states of the metal-to-insulator transition prior to memristive switching. The insights into the Raman phase characteristics show that the peak positions of the A_{1g} Ti-O and E_g Li-O signatures can be used as viable "markers" to associated lithium concentration and the present phase present either as insulating spinel $Li_4Ti_5^{4+}O_{12}$ or conductive rock-salt $Li_7[Ti_2^{4+}Ti_3^{3+}]O_{12}$, owing to observable changes in metal-to-insulator state due to their change in octahedral filling of the 16c Wyckoff structural position which will alter the lithium transport dynamics, Figure 2d. Collectively, the results from independent methods using average and element specific characteristics of Raman, EELS, HRTEM and transport measurements further support the identification of the spinel $Li_4Ti_5O_{12}$ phase, where all the Ti ions are in a Ti^{4+} state only, and the rock-salt $Li_7Ti_5O_{12}$ phase, which has a mixture of Ti^{3+} and Ti^{4+}. More importantly, the incorporation of additional Li$^+$ in a lithium titanate-based film clearly impacts its electronic structure, creating a semi-metallic conductor (from the insulator, $Li_4Ti_5O_{12}$), which could be leveraged in memristive switching devices. Next, we perform tests on the memristive characteristics for the spinel $Li_4Ti_5O_{12}$ and rock-salt $Li_7Ti_5O_{12}$ phases of lithium titanate.

Among the resistive switching metal oxides, lithium oxides, which are widely used in in Li-ion batteries, are attractive for the design of neuromorphic devices as they offer, from a material stand point, an excellent opportunity to control switch dynamics by changing the Li content in the system. The idea of this work is to use to our advantage the unique characteristic of lithium titanate to undergo zero-strain metal–insulator transition, in order to control the conductance, and therefore the available number of states, of solid-state memristors without damaging chemo-mechanical deformation.

We now turn to the memristive switching characteristics of the lithium titanate films, which we define and "set" over the initial lithiation degree of the film to be either in the insulating ($Li_4Ti_5O_{12}$, spinel) or in the metallic state ($Li_7Ti_5O_{12}$, rock salt), Figure 2a and b. Independent on the lithium titanate switching oxide phase, the devices always start in a High Resistance State (HRS, "OFF-state") and, upon applied positive bias they return into a Low Resistance State (LRS, "ON-state"). Reversing the voltage, i.e., negative bias, a transition from the HRS to the LRS is found, giving rise to a bipolar resistive switching mechanism. Two remarkable differences can be observed between the insulating $Li_4Ti_5O_{12}$ and metallic conducting $Li_7Ti_5O_{12}$

**ADVANCED
SCIENCE NEWS**
www.advancedsciencenews.com

**ADVANCED
MATERIALS**
www.advmat.de

in their resistive switching characteristics, namely the resistance ratio and the linearity of the current-voltage profile. While a larger resistance ratio and asymmetric current-voltage profile is obtained for $Li_4Ti_5O_{12}$, a more symmetric current-voltage characteristic is measured for $Li_7Ti_5O_{12}$. Analyzing the kinetic response of both films, we conclude that by increasing the sweep rate one order of magnitude, i.e., to 500 mV s^{-1} (Figure S4 in the Supporting Information), $Li_4Ti_5O_{12}$ cannot respond as fast as $Li_7Ti_5O_{12}$, which shows a stable and reproducible cycling, which is also area-dependent, as shown in Figure S5 on the Supporting Information. Additionally, for both switching materials no electroforming is required, which reduces energy consumption and can result in reduced device variability for artificial synaptic network applications.

To be suitable for analogue computing in future NNs the resistance ratio needs to be high enough to specify distinct synaptic weight values in the neural network,[11] while keeping a highly linear operation to increase accuracy and symmetry for these synaptic weight updates. We test the analogue conductance and HRS/LRS ratio of the lithium titanate switches exposing to train voltage pulses to mimic potentiation and depression of the analogue computing with set pulses of 3.5–5 V and 500 ms width with post sequent reset training pulses of −3.5 to −5 V and 500 ms, **Figure 2**c,d. While the low lithiated $Li_4Ti_5O_{12}$ switching device exhibits a low linearity (between positive and negative pulse trains), the highly lithiated

$Li_7Ti_5O_{12}$ switching device reveals high linearity. Dependent on the original engineered lithiation state of the switching oxide, therefore, one can tailor the artificial neural training response to be either linear or non-linear in conductance. This fact, together with the large HRS/LRS ratios observed, paves the way toward a unique material that could be integrated for either spiking neural networks, where highly non-linearity is desired ($Li_4Ti_5O_{12}$) or deep neural networks, where highly symmetric operation is required ($Li_7Ti_5O_{12}$), by simply altering the Li-concentration in the films at the processing step. We emphasize that all recent reports on lithium oxides 2-terminal switches such as class of lithium cobaltites do predominantly show asymmetric switching response for neural training with no opportunities to modulate the switching characteristic upon lithium phase change in the switching oxide. Analyzing the literature, it may be hypothesized that the complex phase separation behavior of lithium cobaltites[40] (even in single grains of the switch[37]) may not allow the miscibility gap and metal-to-insulator transition to be tuned as precisely as in the material class of lithium titanates.

Another interesting aspect is the change in dynamics depending on the originally set lithium titanate phase of the resistive switch, which may have applications such as controlling the neuron firing time in spiking neural networks. To gain more insights into the dynamics and role of initial film lithiation and metal–insulator characteristics set by processing, we
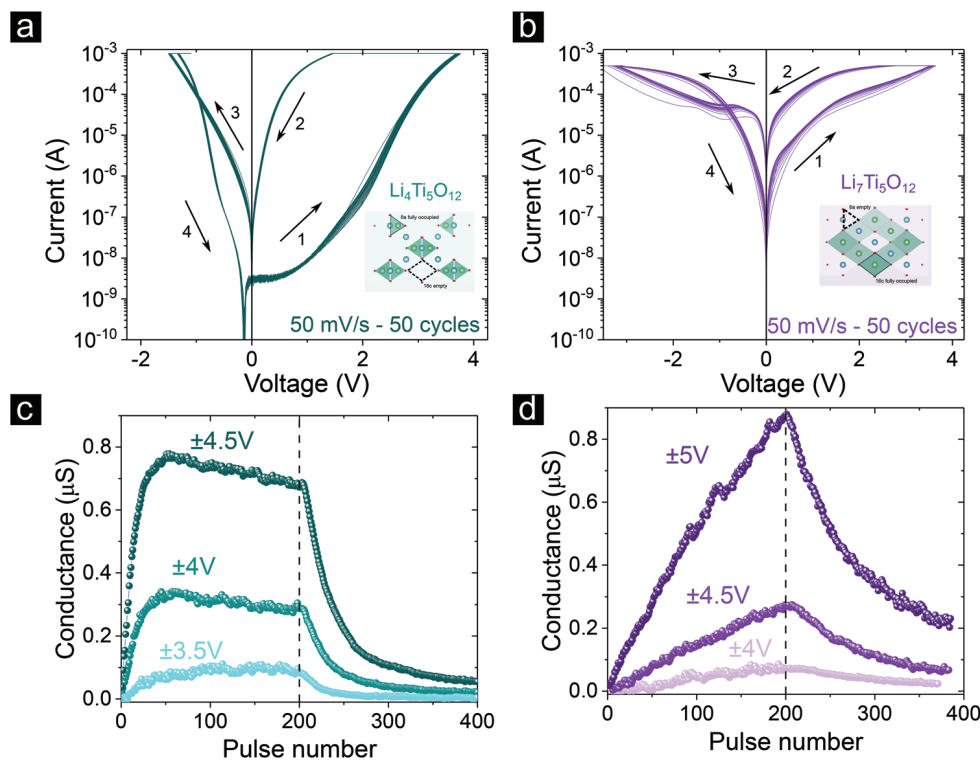

Figure 2. Electrical characterization through cyclic voltammetry and pulsing schemes. a) *I–V* curves in stoichiometric Pt/$Li_4Ti_5O_{12}$/Pt 80 nm-thick film. 50 cycles are shown at a sweep rate of 50 mV s^{-1} on a 500 µm x 500 µm size device. b) *I–V* curves in overlithiated Pt/$Li_7Ti_5O_{12}$/Pt 80 nm-thick film. 50 cycles are shown at a sweep rate of 50 mV s^{-1} on a 500 µm x 500 µm size device. c) Train pulses consisting of 200 positive pulses followed by 200 negative pulses at the voltages specified in the graph with pulse width of 500 ms in a 100 µm by 100 µm size device of stoichiometric Pt/$Li_4Ti_5O_{12}$/Pt 80 nm-thick film. d) Train pulses consisting of 200 positive pulses followed by 200 negative pulses at the voltages specified in the graph with pulse width of 500 ms in a 100 µm by 100 µm size device of stoichiometric Pt/$Li_7Ti_5O_{12}$/Pt 80 nm-thick film.

now turned to low bias chronoamperometry ('electrochemical titration'), **Figure 3**a-b. In essence, this experiment is an extension of the pulsing experiments previously shown, but at lower bias and for longer time spans. The response of the $Li_7Ti_5O_{12}$ memristive bits is fast, needing only some seconds to transition from a regime where the switching event is taking place to a second regime where a stable limiting current is reached at large times, Figure 3b. In contrast, the $Li_4Ti_5O_{12}$ response to the same bias is much slower, Figure 3a. By letting the generated HRS relax (see Figure S6 in the Supporting Information), we could access to the retention times of a state, Figure 3c, and resistance window of the devices, Figure 3d. We have defined the retention of the system as the time at which the current reaches the original HRS value. It is remarkable that the retention has been enhanced by almost a factor of 100, reaching the milestone of 10^5s in the highly lithiated $Li_7Ti_5O_{12}$ film, with a resistance window of two orders of magnitude when compared to the $Li_4Ti_5O_{12}$ film, whose resistance ratio spans over four orders of magnitude. This shows the potential of the highly lithiated phase of $Li_7Ti_5O_{12}$ for DNN applications, given the large retentions and linearity, and the opportunities of low lithiated phase of $Li_4Ti_5O_{12}$ toward SNN applications, due to the shorter retention and large resistance changes.

To clarify the changes of switching symmetry in terms of the lithiation degree, we used in-operando Raman spectroscopy[63] to probe the A_{1g} vibration as a "marker" for titanium-oxygen vibration upon applied external bias, **Figure 4**a. This methodology allows to probe the occupancy of the Wyckoff 8a and 16c structural positions that indicate local changes of the electronic states, and thus indicate metal–insulator transition. By applying +4 V over time, we keep track of the normalized Raman shift as well as of the time evolution of the resistance, which changes from high (insulating phase) to low values (conducting phase), Figure 4b. After imposing the applied potential drop in $Li_4Ti_5O_{12}$, the Raman vibrational frequency of the A_{1g} Ti-O mode (green line) decreases continuously in time from 676 to 673 ± 0.5 cm^{-1}. The shift in the frequency implies the partial reduction of the original Ti^{4+} to Ti^{3+}. However, in the case of $Li_7Ti_5O_{12}$ (purple line), the opposite trend is observed, where the Raman band changes from 665 to 669 ± 0.5 cm^{-1}. Similar to the previous case, this shift in the value of observed frequency reflects the partial oxidation of the reduced Ti^{3+} to Ti^{4+}.

The in-operando Raman spectroscopy-electrochemical titration experiment demonstrates two major points that can lead us to a deeper understanding on the resistive switching mechanism: First, when switching lithium titanate from a high to a low resistance state, the local lithium distribution changes. Second, depending on the initial lithiation state of lithium titanate, the transition metal ions can undergo either reduction or oxidization leading the formation of a Li poor ($Li_4Ti_5O_{12}$) and a Li rich ($Li_7Ti_5O_{12}$) phase. Our experimental findings are in agreement with previous studies in the battery field,[54,61] which demonstrated the two-phase coexistence between $Li_4Ti_5O_{12}$ and $Li_7Ti_5O_{12}$. For low values of Li fractional concentration well below 50%, i.e., $x \ll 0.5$, the insulating phase ($Li_4Ti_5O_{12}$) is expected to dominate, resulting in poor electronic conductance, while for $x \gg 0.5$ the metallic phase ($Li_7Ti_5O_{12}$) should percolate throughout the bulk, leading to a conducting network. For intermediate concentrations, DFT calculations[64] of sample configurations have shown that regions of phase coexistence have high mixed electronic and ionic conductivities. However, such studies do not account for the patterns of driven
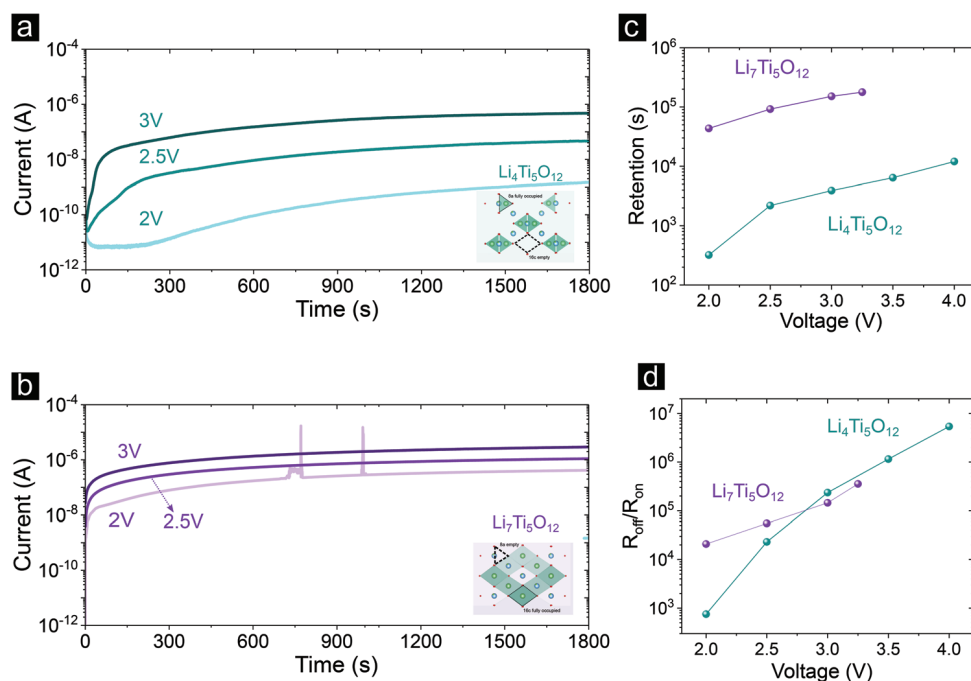

Figure 3. Results of chronoamperometry (Evolution of current with time as a function of bias voltage) experiments measured on the same device (after device reset) for increasing bias voltage on a) Pt/$Li_4Ti_5O_{12}$/Pt (blue lines) and b) Pt/$Li_7Ti_5O_{12}$/Pt (purple lines) 250 μm x 250 μm devices. c) Retention measurements extracted from the current relaxation measurements (see Figure S6 in Supporting Information). d) Resistance window extracted from the retention data.
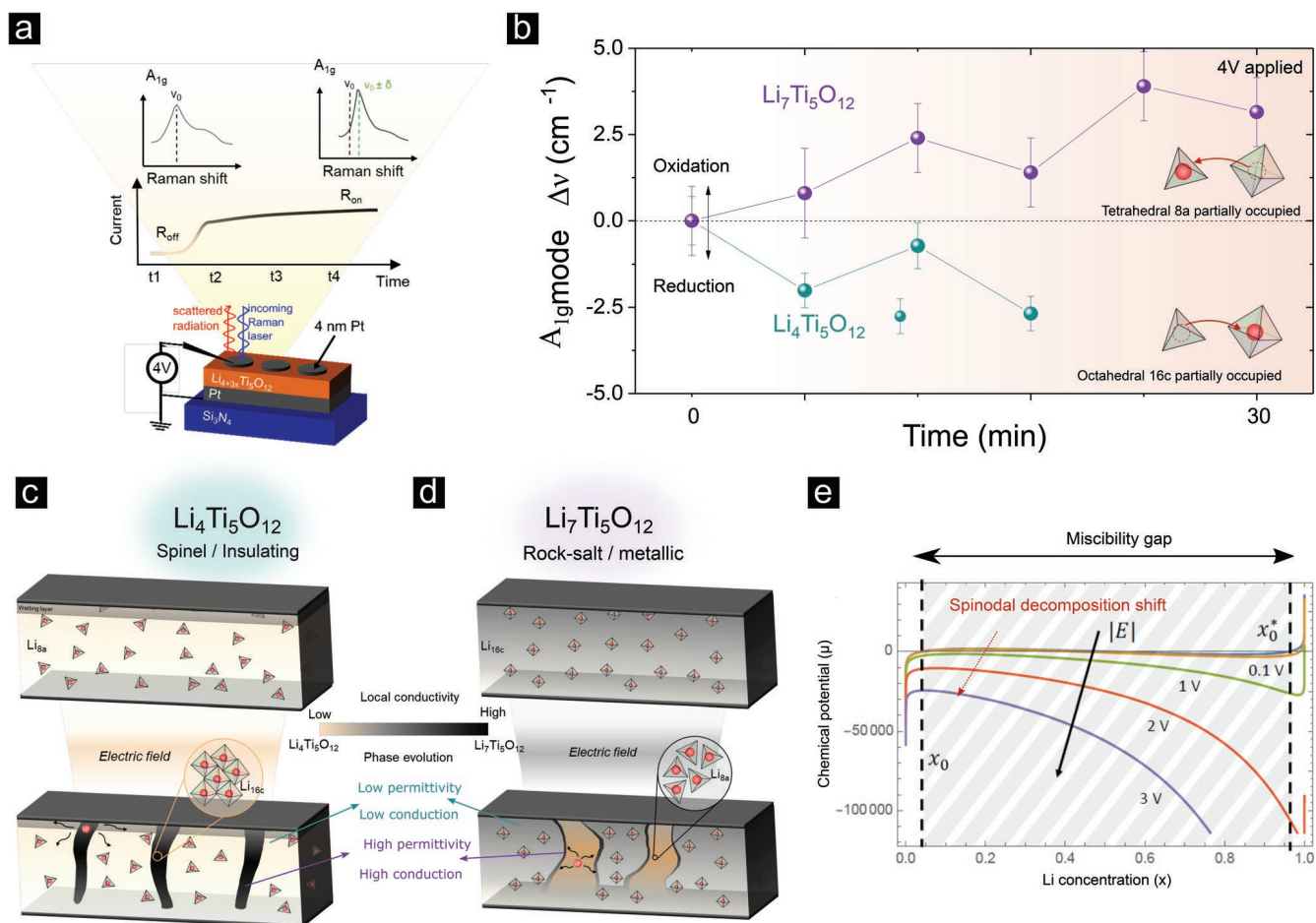
Figure 4. a) Setup and device sketch for in-operando Raman experiments. b) Normalized frequency shift in the A_{1g} Ti–O Raman mode upon applied bias. c) Suggested switching mechanism for $Li_4Ti_5O_{12}$. d) Suggested switching mechanism for $Li_7Ti_5O_{12}$. e) Qualitative plots of original and modified chemical potentials as a function of concentration. Concentration-dependent permittivity shifts the spinodal and binodal points for the metal–insulator phase transition by favoring high Li^+ concentration in regions of high electric field.

phase separation in response to large electric fields, which can strongly influence the observed conductance by effectively placing the metal and insulator phases in series or in parallel between the electrodes.

Based on our experimental findings, combined with the previous experimental and ab initio studies, we propose the existence of an electric-field-dependent miscibility gap for $Li_{4+3x}Ti_5O_{12}$, which modulates the film resistance through electrically driven metal–insulator phase separation. In this physical picture, a homogeneous initial solid solution of lithium ions is driven to phase separate above a critical voltage, leading to the formation of electronically conducting filaments that connect the two metal electrodes, as sketched in Figure 4c,d. Reversing the polarity then destroys the filamentary pattern with a time-delay to allow for redistribution of the lithium concentration, coupled with the evolving electrical current distribution. Voltage cycling leads to reversible creation and destruction of this pattern with hysteresis due to spinodal decomposition of the homogeneous state and nucleation and growth of new phases.

In order to further support our hypothesis and explain the experimental findings, we propose a theoretical model that can describe the electric field-induced phase separation under applied bias, based on electrochemical non-equilibrium thermodynamics.[65] Assuming local electroneutrality in the bulk material (outside thin double layers at the electrode interfaces), the free energy functional for $Li_{4+3x}Ti_5O_{12}$ under an applied potential bias can be expressed in the following general form

$$G[c,\phi] = \int_V \left[g(c,\nabla c) - \frac{1}{2}\varepsilon(c)|\nabla\phi|^2 \right] dV \tag{1}$$

where $0 < c < 1$ is the dimensionless lithium concentration, whose average value is x, and ϕ is the electrostatic potential. The first term in Equation (1) corresponds to the chemical free energy of the inhomogeneous mixture and the second to the electrostatic self-energy that can be stored under the applied potential, which depends on the permittivity $\varepsilon(c)$ as a function of the local lithium content. In the case of the Cahn-Hilliard (or Van der Waals) approximation, $g = g_h(c) + \frac{1}{2}\kappa|\nabla c|^2$, where $g_h(c)$ is the homogeneous free energy density and κ is the gradient penalty. This model has recently been used to describe phase separation in binary fluids,[66] solids,[67,68] and polymers[69–71] driven by applied electric fields. In the case of LTO,

an expression for the chemical part of the free energy has already been developed and parameterized in a recent phase-field model for Li-ion battery simulations,[55] also including electrochemical intercalation reactions and polaron diffusion, but neglecting large electric fields within the active material, which become important in the new application to neuromorphic computing.

Here, we model resistive switching in LTO as a metal–insulator transition, controlled by electrically driven phase separation in a strain-free binary solid. The permittivity of LTO increases with lithium concentration[72] from $\epsilon_i = \epsilon(0) \approx 1.5\ \epsilon_0$ in the insulating phase at room temperature[73] to diverging values in the metallic phase, $\epsilon(c) \to \epsilon_m \gg \epsilon_0$ as $c \to 1$. At low concentration, the permittivity increases roughly in proportion to the population of $Li^+ - e^-$ polaron pairs and then grows nonlinearly with increasing lithium concentration. A simple formula capturing this behavior, based on the Clausius-Mossotti factor for a random packing of polarizable spheres, was first suggested by Herzfeld[74,75]

$$\frac{\epsilon(c)}{\epsilon_i} = \frac{\epsilon_m(1+2c)+2\epsilon_i(1-c)}{\epsilon_m(1-c)+\epsilon_i(2+c)} \sim \frac{1+2c}{1-c} \quad \text{for} \quad \epsilon_m \gg \epsilon_i \tag{2}$$

which diverges in the approach to the metallic phase. This generic behavior of the permittivity has profound consequences for the electrical control of thermodynamic stability, since the total free energy, Equation (1), is lowered by co-locating regions of high lithium concentration with those of high electric field intensity. Above a critical field intensity, this thermodynamic driving force leads to the spontaneous formation of high-permittivity filamentary patterns of lithium ions of connecting the electrodes, which are also short-circuit paths of high conductivity that switch the film resistance.

Starting from a homogeneous initial state, metal–insulator phase separation can occur either by linear instability (spinodal decomposition) or by nucleation and growth from defects or the electrode interfaces. For the general model, Equation (1), the diffusional electrochemical potential of lithium ions can expressed as[65]

$$\mu = \frac{\delta G}{\delta c} = \frac{\delta g}{\delta c} - \frac{1}{2}\epsilon'(c)|\nabla\phi|^2 \tag{3}$$

where the first term is variational derivative of the chemical part of the free energy, which takes the form, $\frac{\delta g}{\delta c} = g_h'(c) - \kappa\nabla^2 c$, in the Cahn-Hilliard approximation. The Gibbs criterion for linear stability requires a convex free energy, $\frac{\delta^2 G}{\delta c^2} > 0$, which can be generalized to account for electrochemical reactions driving electrical current through the system,[76] as in our case of applied voltage bias. The spinodal points, which bound the range of unstable homogeneous concentrations, are thus given by

$$\frac{d\mu}{dc} = g_h''(c) - \frac{1}{2}\epsilon''(c)E^2 = 0 \tag{4}$$

where the electric field strength is $E \approx \Delta V/L$ in the case of a uniform thin film of thickness L subject to a voltage ΔV. Spinodal decomposition of the metallic phase occurs above a critical voltage bias

$$\left|\Delta V_c(c)\right| = L\sqrt{\frac{2\ g_h''(c)}{\epsilon''(c)}} \tag{5}$$

leading to patterns of filamentary short circuits after growth of the initial instability. This result already begins to explain the much larger hysteresis in resistive switching in the low concentration film versus the high concentration film in Figure 3, since the Herzfeld formula (2) predicts $\epsilon'' \approx \frac{3}{2}\epsilon_i(1-c)^{-3}$. Assuming comparable values of $g_h''(c) \approx \frac{1}{2}k^2 > 0$ in the stable insulating and metallic phases, the critical voltage for resistive switching scales as $|\Delta V_c(c)| \approx kL\epsilon_i^{-1/2}(1-c)^{3/2}$. We see that the spinodal points move lower than the equilibrium concentrations for values of voltage in the range of ≈ 3–4 V (Fig S8), which is in quantitative agreement with experimental observations (Figure 2b).

At lower voltage bias, where the material is linearly stable to small perturbations, the system can still phase separate by nucleation and growth, as the binodal points shift under the applied bias. The equilibrium concentrations are the roots of the following pair of algebraic equations,

$$g_h'(c_1) - \epsilon'(c_1)\left|\frac{V}{L}\right|^2 = g_h'(c_2) - \epsilon'(c_2)\left|\frac{V}{L}\right|^2$$
$$= \frac{g_h(c_2)-g_h(c)}{c_2-c_1} - \frac{1}{2}\frac{\epsilon(c_2)-\epsilon(c_1)}{c_2-c_1}\left|\frac{V}{L}\right|^2 \tag{6}$$

which are derived from the requirement of equilibrium between the two phases and the common tangent construction, respectively. Above a lower critical voltage bias that solves Equation (6), nucleation can occur at crystal defects or (perhaps more likely) at the electrode surfaces, where interfacial stability is influenced by surface wetting[77] and driven electro-autocatalytic reactions.[76] These non-equilibrium surface phenomena in turn control pattern formation within the bulk thin film,[78] as has recently been observed by in situ, *in operando* X-ray imaging of nano-platelets of lithium iron phosphate, a phase-separating Li-ion battery material.[79,80]

We are now ready to explain the complex resistive switching behavior of our LTO films, at least qualitatively. **Figure 5**e illustrates typical behavior of the chemical potential as a function of lithium concentration under different values of applied electric field. In the first case, where the initial concentration $x = \varepsilon$ is close to the $Li_4Ti_5O_{12}$ concentration ($\varepsilon \to 0$), a large voltage drop is required to shift the nearby spinodal point (red circles) to lower Li concentrations. In this case, there will be a critical applied voltage drop ΔV_c given by Equation (5) where the spinodal point will move to $x = \varepsilon$ and make the homogeneous solid mixture thermodynamically unstable. As a result, there will be a two-phase co-existence where filaments of the high-permittivity, high-conductivity phase ($Li_7Ti_5O_{12}$) will form so as to connect the two metal Pt electrodes, as sketched in Figure 4c. This phenomenon can qualitatively explain why we observe large hysteretic behavior in the current-voltage curves after applying a positive bias in the system in Figure 2a.

When a negative voltage is applied in the $Li_4Ti_5O_{12}$ film, the experimentally measured current shows asymmetric behavior

**ADVANCED
SCIENCE NEWS**

www.advancedsciencenews.com
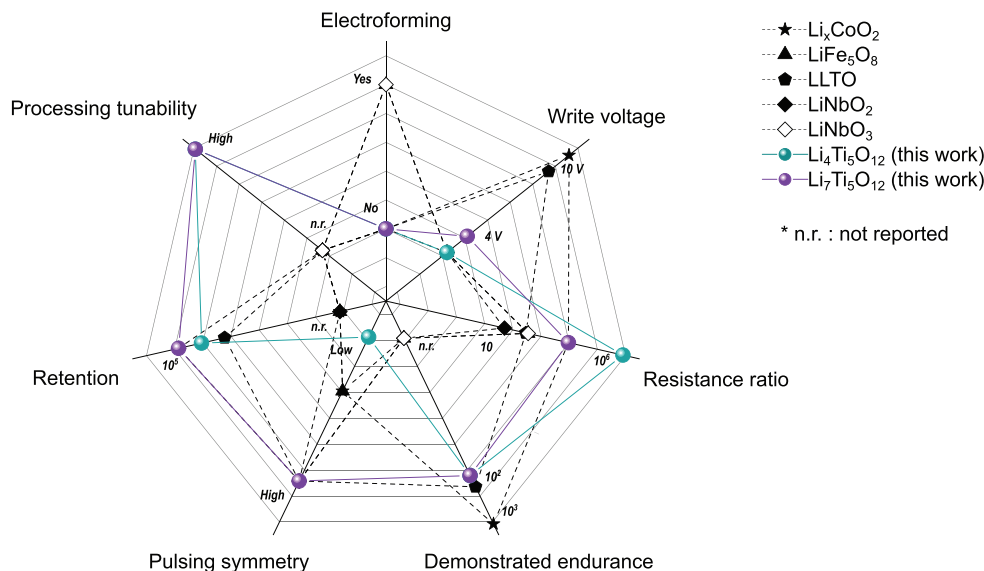
**ADVANCED
MATERIALS**

www.advmat.de

Figure 5. Overview of the different Li-based 2-terminal memristive systems reported so far.

compared to the case of positive applied bias, suggesting that the two electrode interfaces are likely different. Some potential reasons for symmetry breaking in our system are: (i) the manufacturing process leads to a Pt bottom electrode that has been exposed to higher temperatures, while the Pt top electrode is deposited at room temperature; (ii) in similar spinel systems it has been shown that a Li-rich nanometric layer is generated during film preparation,[81] which can cause a thermodynamically favorable state where one of the phases wet the Pt electrode. (iii) the 16d positions are randomly populated by Ti and Li ions with a ratio 5:1, and this is known to affect Li-ion pathways in the bulk.[82] The latter is further supported by Atomic Force Microscopy measurements, in which topography and phase maps show clear contrast between grains, Figure S7. Regardless of the source of broken symmetry between the two Pt/LTO interfaces, it will lead to asymmetry in the current-voltage characteristics. For example, a wetting layer of $Li_7Ti_5O_{12}$ formed on one of the Pt electrodes can become unstable and nucleate phase separation[77] leading to filament formation once sufficiently strong electric field is applied. There will also be asymmetries in the solid-solid electron transfer reaction rates at the two electrode interfaces,[83] which can also directly influence phase separation[76,79,80] and thus the hysteresis in resistive switching.

In the $Li_7Ti_5O_{12}$ device, similar arguments can be made to explain the changes in the current-voltage behavior. The electric field will again induce phase separation by destabilizing $Li_{7-\varepsilon}Ti_5O_{12}$ and lead to the formation of thin insulating domains ($Li_4Ti_5O_{12}$) as well as thick metallic domains ($Li_7Ti_5O_{12}$) in the bulk film, as sketched in Figure 4d. However, the overall lithium content of $Li_7Ti_5O_{12}$ cannot change much upon phase separation, leading to less pronounced changes in the overall conductivity of the device, which remains orders of magnitude large than in the $Li_4Ti_5O_{12}$ device. Assuming as above that $Li_7Ti_5O_{12}$ has larger electric permittivity than $Li_4Ti_5O_{12}$,[72] which diverges in the metallic limit, the applied electric field will induce large asymmetries in the functional form of the

chemical potential, as shown in Figure 4e. In particular, when the device is in the $Li_{7-\varepsilon}Ti_5O_{12}$ state, the voltage required to turn the solution thermodynamically unstable and thus phase separate is smaller than in the case of $Li_{4+\varepsilon}Ti_5O_{12}$, as predicted by the simple spinodal estimate in Equation (5). As noted above, this subtle difference in the permittivity can explain the different hysteretic behavior between the measured current-voltage curves, Figure 3a-b, for $Li_4Ti_5O_{12}$ and $Li_7Ti_5O_{12}$, respectively. The difference in retention can be explained in terms of Li-diffusivity of the phase-separated filament, e.g., the $Li_7Ti_5O_{12}$ filaments created in the $Li_4Ti_5O_{12}$ device would tend to lower retention values, given the higher diffusivity of Li-ions in the $Li_7Ti_5O_{12}$ phase.[51,82] However, at this stage, the size and composition of the filaments remains as an open question, which should be unveiled by advanced characterization techniques.

The conventional wisdom in understanding the transient response of electrochemical materials, such as lithium titanates, to applied voltages is through simple models of diffusion. In the present case, however, we do not change the total Li content, and we only control the electric field and electronic current applied across the device. Therefore, any attempt to understand the physics behind the switching dynamics in terms of classical diffusion of inserted ions, e.g. using the Cottrell equation, will provide false predictions, which is also the case for phase-separating battery materials.[84] Instead, the electric field-induced phase separation of $Li_{4+3x}Ti_5O_{12}$ can be described by electrochemical phase-field models[65,76] in order to understand fundamental physics of resistive switching and engineering design principles for neuromorphic devices.

In summary, the proposed physical picture can qualitatively describe the observed switching behavior of Figure 2 in terms of electric field-induced phase separation, enabled by the dielectric permittivity contrast of $Li_4Ti_5O_{12}$ and $Li_7Ti_5O_{12}$. More specifically, the affinity of inserted lithium ions, which increase the local permittivity, for regions of higher electric field intensity alters the thermodynamic phase diagram out of equilibrium, leading to changes in the binodal and spinodal points of the

solid mixture under applied bias. As a result, a homogeneous film can phase separate into metallic and insulating phases, which form percolating domains between the electrodes. This microscopic picture points toward the development of new criteria for designing lithium based analogue computing devices.

Industrial manufacturing of solid-state battery thin film components and silicon-based electrochemical cells have substantially grown over the last decades and we see potential in generating additional function and use of these materials for future analogue computing hardware. Despite the promise it is to be noted that the field of lithium oxides in neuromorphic computing is young and has still to achieve the maturity level achieved in their O^{2-}, Ag^+/Cu^{2+} and PCM resistive switching counterparts. In particular, it remains unclear the performance that Li-based materials will have in 2-Terminal based neural networks upon material optimization. The ability of lithium oxide materials to use future cell designs with lithium fluxes (microbatteries) to control the synaptic response is attractive and challenging to mimic with current resistive switch hardware designs. For instance, the control of the Metal–Insulator Transition via Li-stoichiometry in the devices directly at processing is an appealing approach to produce very large changes in the device properties and might have a strong impact on 3-Terminal configurations. One key point in the development of battery oxide materials that may also function as synaptic hardware components besides classic energy storage is the knowledge on their phase evolution and stability at given field strength. Our hypothesis and selection criteria for the newly proposed lithium titanate is deeply rooted on phase stability and miscibility gap arguments known in the battery field, but applied to deeply alter synaptic weights through different resistive states by changes in transport dynamics.

To reflect on this more broadly, we give a rough summary of the main properties reported so far for Li-based resistive switches that summarizes the selection criteria based on phase stability that we discussed, Figure 5. The key points of $Li_{4+3x}Ti_5O_{12}$ systems when compared to other tested Li-based oxide memristors (e.g., Li_xCoO_2, $LiFe_5O_8$, $LiLaTiO_3$, $LiNbO_2$ and $LiNbO_3$) rely on the absence of electroforming, low voltage operation, large resistance ratios without the need of exchange with a silicon scavenging layer (which is the case for Li_xCoO_2) and tunable retention. Our work makes a strong point for the ability to tune the performance of the devices upon controlling the Lithiation degree in the films, that, even though it is a novel process in terms of processing as well, it might result easier than oxygen-control on the long run. Lithiation degree could become an extra knob to further tune and control the memristive properties of Li-based devices. We also clearly demonstrate by computation and experimental evidences that the phase miscibility gap in lithium titanates is unique among the tested lithium-based memristor and is the key to widely alter the synaptic characteristics, which could either later be tailored for DNN or SNN applications on demand. These facts pose lithium titanates in a unique position of widespread use of different types of neural networks given the ability to tune their performance, which has not been the case for any other lithium-based memristive system so far.

Lithium-ion battery electrode materials have the potential for surprising new uses beyond simply energy storage, such

as providing functional materials for neuromorphic analogue computing. Through their spinel, layered and rock salt structures, various material classes of cobaltites, titanates or ferrates are able to use intercalated lithium as a knob to turn metal-to-insulator transitions on and off. Despite the potential of these material classes for additional functionalities beyond their use in batteries, to date there have emerged no selection criteria or design rules for such uses. Rational design of devices using these materials will eventually require detailed analysis of electrochemical reactions and phase behavior under the high electric fields required for neuromorphic computing.

As a first step, here we have exploited the thermodynamic properties of a well-known battery anode material, lithium titanate, to perform resistive switching by electrically controlling metal-to-insulator phase separation, with a negligible volume change in "zero-strain" solid phase separation. One of the most striking outcomes is that the metal–insulator transition can be conveniently modulated for neuromorphic computing purposes, such as control of the neural pulse train symmetry and linearity in conductance and the resistance on-to-off ratio, simply by adjusting the lithium stoichiometry and phase pattern. We demonstrate by combined ex- and in-operando Raman spectroscopy, electron microscopy and electrochemical methods that the filling and emptying of the Wyckoff 16c structural position with lithium is the knob to turn to set the desired reversible resistive-switching characteristics of titanate thin films.

A simple phase-field theory considering the lithium concentration-dependent permittivity and conductivity is able to explain the current-voltage transients in terms of electrostatic self-energy changes, which shift the spinodal and binodal points for the stability of metal–insulator phase separation. This is consistent with the local modulation of the lithiation degree between 8a and 16c Wyckoff positions generating highly conducting percolative paths and paves the way for quantitative modeling and design of LTO based memristive devices. Our understanding of phase evolution, stability regimes and lithium dynamics the from battery field thus could enable predictions of which metal-to-insulator phase behavior is best suited in specific device geometries for lithium-controlled neuromorphic computing.

In summary, we show that lithium titanates (state-of-the-art battery anodes) have unique functionality for fast resistive switching based on zero-strain metal–insulator phase separation, which can be easily tuned for a specific application. Lithium stoichiometry can be reversibly adjusted within a single hardware material, for example, to alter the linearity of a pulse train for analogue computing, to tune asymmetric switching with low retention for two-terminal spiking neural networks, or to enable linear and more symmetric switching with high retention for deep neural networks. The interdisciplinary nature of this work may open new directions for chemists, material scientists and hardware engineers to systematically design phases and carrier dynamics for specific neuromorphic architectures and output functions, thus increasing the value chain and introducing dual uses of familiar battery materials as analogue computational circuit elements. Microbatteries are well established in industry and have successfully been integrated in silicon-based chips, so this perspective may

lead to lithium oxide-based computer hardware using similar material classes and manufacturing routes as for microbattery components.

Conflict of Interest

The authors declare no conflict of interest.

Author Contributions

J.C.G.-R. and J.L.M.R. proposed the concepts and designed the experiments. J.C.G.-R., M.B., and K.M.M. carried out the experiments. Z.H. performed the electron microscopy measurements. J.C.G.-R. and R.P. prepared the PLD targets and designed the methodology for film preparation. N.N., D.F., and M.Z.B. designed and performed the computational analysis. J.C.G.-R., M.B., Z.H., N.N., K.K., M.Z.B., and J.L.M.R. performed the analysis of the data. J.C.G.-R., N.N., D.F., M.Z.B., and J.L.M.R. wrote the manuscript with help of all of the co-authors.

[1] L. Chua, *IEEE Trans. Circuit Theory* **1971**, *CT-18*, 507.
[2] T. W. Hickmott, *J. Appl. Phys.* **1962**, *33*, 2669.
[3] J. F. Gibbons, W. E. Beadle, *Solid-State Electron.* **1964**, *7*, 785.
[4] R. Waser, M. Aono, *Nat. Mater.* **2007**, *6*, 833.
[5] R. Waser, R. Dittmann, G. Staikov, K. Szot, *Adv. Mater.* **2009**, *21*, 2632.
[6] J. J. Yang, D. B. Strukov, D. R. Stewart, *Nat. Nanotechnol.* **2013**, *8*, 13.
[7] A. A. Chien, V. Karamcheti, *Computer (Long Beach Calif)*. **2013**, *46*, 48.
[8] A. Sebastian, M. Le Gallo, G. W. Burr, S. Kim, M. Brightsky, E. Eleftheriou, *J. Appl. Phys.* **2018**, *124*, 111101.
[9] S. Ambrogio, P. Narayanan, H. Tsai, R. M. Shelby, I. Boybat, C. Di Nolfo, S. Sidler, M. Giordano, M. Bodini, N. C. P. Farinha, B. Killeen, C. Cheng, Y. Jaoudi, G. W. Burr, *Nature* **2018**, *558*, 60.
[10] M. Prezioso, F. Merrikh-Bayat, B. D. Hoskins, G. C. Adam, K. K. Likharev, D. B. Strukov, *Nature* **2015**, *521*, 61.
[11] T. Gokmen, Y. Vlasov, *Front. Neurosci.* **2016**, *10*, 333.
[12] F. Pan, S. Gao, C. Chen, C. Song, F. Zeng, *Mater. Sci. Eng.: R Rep.* **2014**, *83*, 1.
[13] G. W. Burr, B. N. Kurdi, J. C. Scott, C. H. Lam, K. Gopalakrishnan, R. S. Shenoy, *IBM J. Res. Dev.* **2008**, *52*, 449.
[14] A. Wedig, M. Luebben, M. Moors, D. Y. Cho, K. Skaja, T. Hasegawa, K. K. Adepalli, B. Yildiz, R. Waser, I. Valov, *Nat. Nanotechnol.* **2015**, *11*, 67.
[15] J. J. Yang, M. D. Pickett, X. Li, D. A. A. Ohlberg, D. R. Stewart, R. S. Williams, *Nat. Nanotechnol.* **2008**, *3*, 429.
[16] M. J. Lee, C. B. Lee, D. Lee, S. R. Lee, M. Chang, J. H. Hur, Y. B. Kim, C. J. Kim, D. H. Seo, S. Seo, U. I. Chung, I. K. Yoo, K. Kim, *Nat. Mater.* **2011**, *10*, 625.
[17] M. Kubicek, R. Schmitt, F. Messerschmitt, J. L. M. Rupp, *ACS Nano* **2015**, *9*, 10737.
[18] R. Schmitt, J. Spring, R. Korobko, J. L. M. Rupp, *ACS Nano* **2017**, *11*, 8881.
[19] S. Schweiger, R. Pfenninger, W. J. Bowman, U. Aschauer, J. L. M. Rupp, *Adv. Mater.* **2017**, *29*, 1605049.
[20] R. Schmitt, M. Kubicek, E. Sediva, M. Trassin, M. C. Weber, A. Rossi, H. Hutter, J. Kreisel, M. Fiebig, J. L. M. Rupp, *Adv. Funct. Mater.* **2019**, *29*, 1804782.
[21] F. Messerschmitt, M. Kubicek, S. Schweiger, J. L. M. Rupp, *Adv. Funct. Mater.* **2014**, *24*, 7448.
[22] K. Hoshino, N. L. Peterson, C. L. Wiley, *J. Phys. Chem. Solids* **1985**, *46*, 1397.
[23] R. Nakamura, T. Toda, S. Tsukui, M. Tane, M. Ishimaru, T. Suzuki, H. Nakajima, *J. Appl. Phys.* **2014**, *116*, 033504.
[24] H. Jiang, D. A. Stewart, *J. Appl. Phys.* **2016**, *119*, 134502.
[25] I. Valov, R. Waser, J. R. Jameson, M. N. Kozicki, *Nanotechnology* **2011**, *22*, 254003.
[26] N. Banno, T. Sakamoto, T. Hasegawa, K. Terabe, M. Aono, *Jpn. J. Appl. Phys., Part 1* **2006**, *45*, 3666.
[27] M. N. Kozicki, M. Park, M. Mitkova, *IEEE Trans. Nanotechnol.* **2005**, *4*, 331.
[28] C. Schindler, M. Weides, M. N. Kozicki, R. Waser, *Appl. Phys. Lett.* **2008**, *92*, 122910.
[29] M. N. Kozicki, H. J. Barnaby, *Semicond. Sci. Technol.* **2016**, *31*, 113001.
[30] K. Terabe, T. Hasegawa, T. Nakayama, M. Aono, *Nature* **2005**, *433*, 47.
[31] Y. Li, W. C. Chueh, *Annu. Rev. Mater. Res.* **2018**, *48*, 137.
[32] H. Xia, L. Lu, G. Ceder, *J. Power Sources* **2006**, *159*, 1422.
[33] B. Stanje, D. Rettenwander, S. Breuer, M. Uitz, S. Berendts, M. Lerch, R. Uecker, G. Redhammer, I. Hanzu, M. Wilkening, *Ann. Phys.* **2017**, *529*, 1700140.
[34] J. van den Broek, S. Afyon, J. L. M. Rupp, *Adv. Energy Mater.* **2016**, *6*, 1.
[35] A. Milewska, K. Świerczek, J. Tobola, F. Boudoire, Y. Hu, D. K. Bora, B. S. Mun, A. Braun, J. Molenda, *Solid State Ionics* **2014**, *263*, 110.
[36] A. Moradpour, O. Schneegans, S. Franger, A. Revcolevschi, R. Salot, P. Auban-Senzier, C. Pasquier, E. Svoukis, J. Giapintzakis, O. Dragos, V. C. Ciomaga, P. Chrétien, *Adv. Mater.* **2011**, *23*, 4141.
[37] X. Zhu, C. S. Ong, X. Xu, B. Hu, J. Shang, H. Yang, S. Katlakunta, Y. Liu, X. Chen, L. Pan, J. Ding, R.-W. Li, *Sci. Rep.* **2013**, *3*, 1084.
[38] V. H. Mai, A. Moradpour, P. A. Senzier, C. Pasquier, K. Wang, M. J. Rozenberg, J. Giapintzakis, C. N. Mihailescu, C. M. Orfanidou, E. Svoukis, A. Breza, C. B. Lioutas, S. Franger, A. Revcolevschi,

T. Maroutian, P. Lecoeur, P. Aubert, G. Agnus, R. Salot, P. A. Albouy, R. Weil, D. Alamarguy, K. March, F. Jomard, P. Chrétien, O. Schneegans, *Sci. Rep.* **2015**, *5*, 7761.

[39] V. S. Nguyen, V. H. Mai, P. A. Senzier, C. Pasquier, K. Wang, M. J. Rozenberg, N. Brun, K. March, F. Jomard, J. Giapintzakis, C. N. Mihailescu, E. Kyriakides, P. Nukala, T. Maroutian, G. Agnus, P. Lecoeur, S. Matzen, P. Aubert, S. Franger, R. Salot, P. Albouy, D. Alamarguy, B. Dkhil, P. Chrétien, O. Schneegans, *Small* **2018**, *14*, 1801038.

[40] N. Nadkarni, T. Zhou, D. Fraggedakis, T. Gao, M. Z. Bazant, *Adv. Funct. Mater.* **2019**, *29*, 1902821.

[41] X. Zhu, J. Zhou, L. Chen, S. Guo, G. Liu, R. W. Li, W. D. Lu, *Adv. Mater.* **2016**, *28*, 7658.

[42] C. M. Orfanidou, P. S. Ioannou, E. Kyriakides, C. Nicolaou, C. N. Mihailescu, V. S. Nguyen, V. H. Mai, O. Schneegans, J. Giapintzakis, *AIP Adv.* **2018**, *8*, 115211.

[43] J. D. Greenlee, C. F. Petersburg, W. Laws Calley, C. Jaye, D. A. Fischer, F. M. Alamgir, W. Alan Doolittle, *Appl. Phys. Lett.* **2012**, *100*, 182106.

[44] C. Yakopcic, S. Wang, W. Wang, E. Shin, J. Boeckl, G. Subramanyam, T. M. Taha, *Neural Comput. Appl.* **2018**, *30*, 3773.

[45] J. D. Greenlee, J. C. Shank, M. B. Tellekamp, E. X. Zhang, J. Bi, D. M. Fleetwood, M. L. Alles, R. D. Schrimpf, W. A. Doolittle, *IEEE Trans. Nucl. Sci.* **2013**, *60*, 4555.

[46] S. Wang, W. Wang, C. Yakopcic, E. Shin, G. Subramanyam, T. M. Taha, *Microelectron. Eng.* **2017**, *168*, 37.

[47] T. Shi, J. F. Wu, Y. Liu, R. Yang, X. Guo, *Adv. Electron. Mater.* **2017**, *3*, 1700046.

[48] K. Mukai, Y. Kato, H. Nakano, *J. Phys. Chem. C* **2014**, *118*, 2992.

[49] B. Zhao, R. Ran, M. Liu, Z. Shao, *Mater. Sci. Eng.: R Rep.* **2015**, *98*, 1.

[50] K. M. Colbow, J. R. Dahn, R. R. Haering, *J. Power Sources* **1989**, *26*, 397.

[51] W. Schmidt, P. Bottke, M. Sternad, P. Gollob, V. Hennige, M. Wilkening, *Chem. Mater.* **2015**, *27*, 1740.

[52] M. Wagemaker, D. R. Simon, E. M. Kelder, J. Schoonman, C. Ringpfeil, U. Haake, D. Lützenkirchen-Hecht, R. Frahm, F. M. Mulder, *Adv. Mater.* **2006**, *18*, 3169.

[53] X. Lu, L. Zhao, X. He, R. Xiao, L. Gu, Y. S. Hu, H. Li, Z. Wang, X. Duan, L. Chen, J. Maier, Y. Ikuhara, *Adv. Mater.* **2012**, *24*, 3233.

[54] D. Young, A. Ransil, R. Amin, Z. Li, Y.-M. Chiang, *Adv. Energy Mater.* **2013**, *3*, 1125.

[55] A. Vasileiadis, N. J. J. de Klerk, R. B. Smith, S. Ganapathy, P. P. R. M. L. Harks, M. Z. Bazant, M. Wagemaker, *Adv. Funct. Mater.* **2018**, *28*, 1705992.

[56] R. Pfenninger, M. Struzik, I. Garbayo, E. Stilp, J. L. M. Rupp, *Nat. Energy* **2019**, *4*, 475.

[57] F. Ronci, P. Reale, B. Scrosati, S. Panero, V. R. Albertini, P. Perfetti, M. di Michiel, J. M. Merino, *J. Phys. Chem. B* **2002**, *106*, 3082.

[58] D. V. Pelegov, B. N. Slautin, V. S. Gorshkov, P. S. Zelenovskiy, E. A. Kiselev, A. L. Kholkin, V. Y. Shur, *J. Power Sources* **2017**, *346*, 143.

[59] T.-F. Yi, S.-Y. Yang, Y. Xie, *J. Mater. Chem. A* **2015**, *3*, 5750.

[60] I. a. Leonidov, O. N. Leonidova, L. a. Perelyaeva, R. F. Samigullina, S. a. Kovyazina, M. V. Patrakeev, *Phys. Solid State* **2003**, *45*, 2183.

[61] M. G. Verde, L. Baggetto, N. Balke, G. M. Veith, J. K. Seo, Z. Wang, Y. S. Meng, *ACS Nano* **2016**, *10*, 4312.

[62] D. G. Kellerman, V. S. Gorshkov, E. V. Shalaeva, B. A. Tsaryev, E. G. Vovkotrub, *Solid State Sci.* **2012**, *14*, 72.

[63] E. Sediva, T. Defferriere, N. H. Perry, H. L. Tuller, J. L. M. Rupp, *Adv. Mater.* **2019**, *31*, 1902493.

[64] S. Ganapathy, A. Vasileiadis, J. R. Heringa, M. Wagemaker, *Adv. Energy Mater.* **2017**, *7*, 1601781.

[65] M. Z. Bazant, *Acc. Chem. Res.* **2013**, *46*, 1144.

[66] M. D. Johnson, X. Duan, B. Riley, A. Bhattacharya, W. Luo, *Phys. Rev. E* **2004**, *69*, 041501.

[67] W. Hong, K. C. Pitike, *Procedia IUTAM* **2015**, *12*, 73.

[68] K. Chaitanya Pitike, W. Hong, *J. Appl. Phys.* **2014**, *115*, 044101.

[69] Z. H. Shen, J. J. Wang, J. Y. Jiang, S. X. Huang, Y. H. Lin, C. W. Nan, L. Q. Chen, Y. Shen, *Nat. Commun.* **2019**, *10*, 1843.

[70] S. Orizaga, K. Glasner, *Phys. Rev. E* **2016**, *93*, 052504.

[71] N. Gavish, I. Versano, A. Yochelis, *SIAM J. Appl. Dyn. Syst.* **2017**, *16*, 1946.

[72] Y. Liu, J. Lian, Z. Sun, M. Zhao, Y. Shi, H. Song, *Chem. Phys. Lett.* **2017**, *677*, 114.

[73] B. Vikram Babu, K. Vijaya Babu, G. Tewodros Aregai, L. Seeta Devi, B. Madhavi Latha, M. Sushma Reddi, K. Samatha, V. Veeraiah, *Results Phys.* **2018**, *9*, 284.

[74] K.F. Herzfeld, *Phys. Rev.* **1927**, *29*, 701.

[75] K.-F. Berggren, *J. Chem. Phys.* **1974**, *60*, 3399.

[76] M. Z. Bazant, *Faraday Discuss.* **2017**, *199*, 423.

[77] D. A. Cogswell, M. Z. Bazant, *Nano Lett.* **2013**, *13*, 3036.

[78] N. Nadkarni, E. Rejovitsky, D. Fraggedakis, C. V. Di Leo, R. B. Smith, P. Bai, M. Z. Bazant, *Phys. Rev. Mater.* **2018**, *2*, 085406.

[79] J. Lim, Y. Li, D. H. Alsem, H. So, S. C. Lee, P. Bai, D. A. Cogswell, X. Liu, N. Jin, Y. S. Yu, N. J. Salmon, D. A. Shapiro, M. Z. Bazant, T. Tyliszczak, W. C. Chueh, *Science* **2016**, *353*, 566.

[80] P. Bai, D. A. Cogswell, M. Z. Bazant, *Nano Lett.* **2011**, *11*, 4890.

[81] S. Mesoraca, J. E. Kleibeuker, B. Prasad, J. L. MacManus-Driscoll, M. G. Blamire, *J. Cryst. Growth* **2016**, *454*, 134.

[82] B. Ziebarth, M. Klinsmann, T. Eckl, C. Elsässer, *Phys. Rev. B: Condens. Matter Mater. Phys.* **2014**, *89*, 174301.

[83] P. Bai, M. Z. Bazant, *Nat. Commun.* **2014**, *5*, 3585.

[84] G. K. Singh, G. Ceder, M. Z. Bazant, *Electrochim. Acta* **2008**, *53*, 7599.